Dynamic behaviour and stability analysis of a compensated aerostatic pad

Dynamic behaviour and stability analysis of a compensated aerostatic pad

*Federic*o Colombo, *Luigi* Lentini, *Terenziano* Raparelli, *Andrea* Trivella*, *Vladimir* Viktorov

Politecnico di Torino, C.so Duca degli Abruzzi 24, 10129, Torino, Italy

Abstract. Thanks to their low friction, aerostatic pads have important applications in precision positioning systems and linear guides. A simple and cheap solution to increase the static stiffness of aerostatic pads is to add a proper designed pneumatic valve to regulate the air flow supplied to the bearing. However, integrating aerostatic pads with additional devices can reduce its dynamic performance. This paper presents a numerical study on the dynamic behaviour and stability a commercial aerostatic pad controlled by a custom-built diaphragm valve. The bearing performance is studied by means of a lumped parameters model. Air bearing stiffness and damping are analysed in the frequency domain. Subsequently, the lumped model is linearized to investigate the stability of the system by means of Routh-Hurwitz method. The performance of the controlled air pad is compared to that of a simple commercial air pad.

1 Introduction

Aerostatic bearings are commonly used in applications that require high positioning accuracy. Due to their relative low stiffness, various solutions are used to improve the performance of these devices [1,2]. The use of multiple orifices [3–5], compound restrictors [6], microholes [7] and porous surfaces [8,9] as feeding system are possible solutions to increase the stiffness and load capacity of air pads. Moreover, stiffness can be further improved by using suitable active or passive compensation systems [10,11]. Active compensation systems can lead to significant performance improvement, but, due to the need for sensors, actuators and controllers, they represent an expensive solution. Conversely, despite their limited performance improvements, passive compensation systems are a cheaper alternative solutions than may be employed for industrial applications. Ghodsiyeh et al. [12] have proposed a passive compensation method consisting in the integration of an aerostatic pad and a diaphragm valve.

It was found numerically and experimentally that this kind of compensation makes it possible to obtain bearings with quasi-infinite and even negative static stiffness.

* Corresponding author: andrea.trivella@polito.it

Experimental tests confirmed that a negative stiffness does not imply the presence of dynamic instability, but it is due to the overcompensation of the diaphragm valve. However, these analyses made not possible to define the stability threshold of the system and how the stability is related to the bearing design parameters.

This paper presents a numerical study of the dynamic behavior of the compensated pad using the lumped parameter model. Stiffness and damping are investigated using the perturbation method. Additionally, Routh-Hurwitz method is used to study stability of the linearized model of the pad. The performance of the here proposed system is compared to a commercial air pad used as a benchmark.

2 Aerostatic pad description

Figure 1a shows the geometry of the compensated air pad. The pad has a rectangular base (A= 60 mm and B=30 mm) and four orifices of diameter d=1 mm. The orifices are located in the middle of the sides of a rectangular groove line of dimensions a= 45 mm and b=20 mm. Figure 1b shows the cross-section of the feeding hole. The groove presents a triangular cross-section of height h_g= 60 μm and with w_g = 200 μm. The performance of the compensated pad is compared to that of a commercial pad of same shape, size and groove but with four holes of diameter 0.18mm. Moreover, the commercial pad has conical pockets downstream from each supply hole with a depth of 300 μm and a diameter of 0.8 mm. The reason of the different supply hole diameter is due to the presence of the regulating valve. To make the regulation more effective, it is convenient to reduce the pneumatic resistance of the supply holes of the compensated pad compared to that of the supply hole of the valve nozzle.

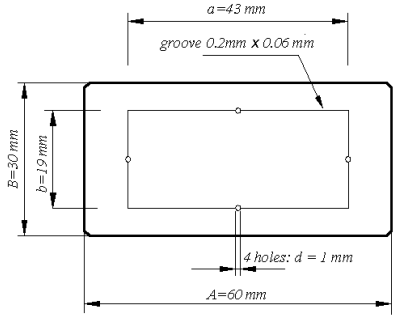

Fig. 1a. Compensated air pad.

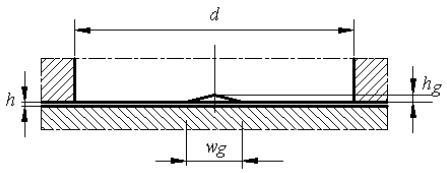

Fig. 1b. Supply hole cross geometry.

3 Diaphragm valve

Fig. 2 illustrates the scheme of the nozzle of the custom-built diaphragm valve. Compressed air is supplied to the valve at the absolute pressure P_S, passes through the nozzle (1) and it is exhausted from its diameter d_V = 0.5 mm. The diaphragm (2) is a circular steel foil of diameter D = 6 mm and stiffness k_m = 180 N/mm. P_1 is the absolute pressure in the control chamber of the valve, P_a is the ambient pressure. When $P_1 = P_a$, the diaphragm is undeformed (dotted line) and the initial distance x_0 between the nozzle and the diaphragm can be manually regulated through a micrometric screw. On this regard, it was experienced

that the compensating action of the valve is more efficient when, in the absence of air supply, the diaphragm is initially preloaded by the nozzle, i.e., for negative values of x_0.

The bending of the diaphragm preloaded by the nozzle causes the passage of a small air flow. The nozzle-diaphragm distance corresponding to the minimum flow rate passing through the valve has been identified with an equivalent distance $x_{min} = 12\ \mu m$.

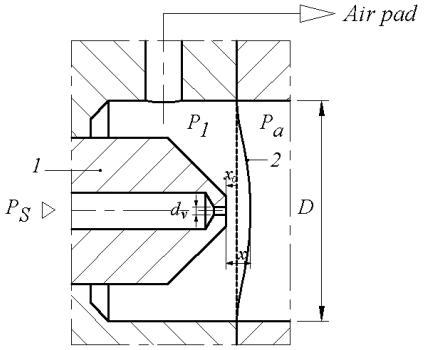

Fig. 2. Scheme of the control valve: enlargement of diaphragm and nozzle

4 Mathematical lumped model

The surface of the pad and the counter pad are assumed parallel and perfectly smooth. Figure 3 shows the pneumatic scheme of the system. It consists of a series of lumped pneumatic resistances and volumes. R_1 is the resistance of the nozzle-diaphragm, R_2 corresponds to the resistance of each supply hole of the pad, R_3 is the viscous resistance due to the air gap height h of the pad. V_1 corresponds to the volumes of the supply duct of the pad, V_0 is the sum of the air gap volume $A\ B\ h$ and groove volumes V_g ($V_0 = A\ B\ h + V_g$).

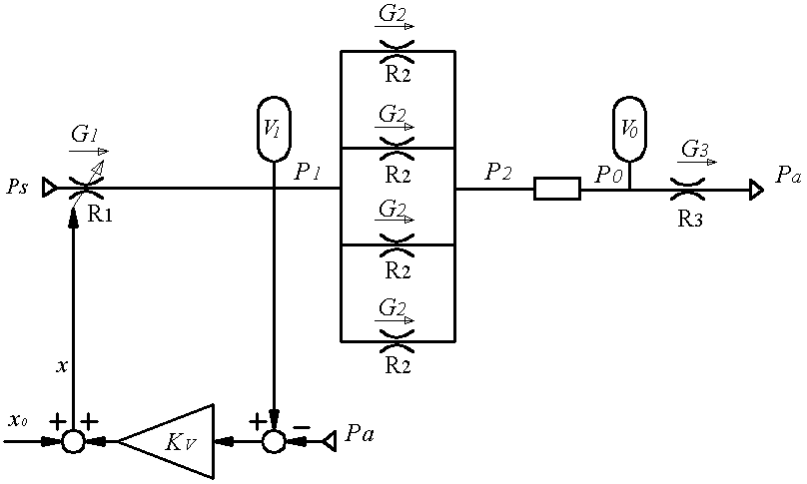

Fig. 3. Pneumatic scheme of the compensated air pad with the diaphragm pneumatic valve.

The distance x between nozzle and diaphragm is a linear function of the pressure P_1:

$$x = x_0 + k_V\,(P_1 - P_a)\,;\; k_V = \frac{\pi D^2}{4k_m} \tag{1}$$

P_2 is the absolute pressure immediately downstream each pad orifice. The mass flow through the first two resistances R_i (i = 1, 2) is described by the ISO formula 6358:

$$G_i = \sqrt{T_0/T}\; C_i\, P_i \sqrt{1-\varphi_i{}^2}\,;\; \varphi_i = \frac{(P_d/P_u) - b_c}{1 - b_c} \tag{2}$$

where φ_i represents subsonic ($0 < \varphi_i \leq 1$) or sonic ($\varphi_i = 0$) conditions, P_u, P_d are the upstream and downstream absolute pressures of each resistance, b_c is the pressure critical ratio, assumed equal to 0.528. T_0 and T are a reference ($T_0 = 293$ K) and the environmental air temperatures. C_i is the conductance of the ith cross-section. The expression of C_2 takes into account the presence of the grooves crossing the pockets:

$$C_1 = \psi\, c_{d_{a,1}} \pi\, d_V\, x\,;\;\; C_2 = \psi\, c_{d_{a,2}} \left(\pi\, d\, h + w_g\, h_g\right) \tag{3}$$

where ψ =$0.686/\sqrt{R\,T}$, R = 287 J kg-1 K, and $c_{da,i}$ (i = 1, 2) are the discharge coefficients at the nozzle and pad holes outlet, which were experimentally obtained in [13]:

$$c_{da,i} = 1.05\,(1 - 0.3\,\mathrm{e}^{-0.005\,Re_i});$$

$$Re_1 = \frac{G_1}{\pi \mu d_V};\; Re_2 = \frac{G_2\, h}{\pi\, \mu d h_{eq}}\,;\; h_{eq} = \frac{\pi d\, h + w_g\, h_g}{\pi d} \tag{4}$$

where Re_i is the Reynolds number. The pressure distribution was computed on the basis of the 2D Reynolds equation under isothermal conditions:

$$\frac{dP}{dx} + 12\mu RT\,\frac{g_x}{Ph^3} = 0;\; \frac{dP}{dy} + 12\mu RT\,\frac{g_y}{Ph^3} = 0 \tag{5}$$

where g_x and g_y are the mass flow rates per unit of width along the x and y directions and μ is the air dynamic viscosity. The mass flow rates G_x and G_y, outgoing from each side of the rectangular groove are obtained by integration of the Reynolds equations. The total air consumption G of the pad is obtained as follows:

$$G = G_3 = 2(G_x + G_y) = \frac{1}{6\mu RT}\upsilon\,(P_0^2 - P_a^2)h^3;$$
$$\upsilon = \left(\frac{b}{A-a} + \frac{a}{B-b}\right) \tag{6}$$

The model assumes a constant pressure P_0 under the rectangular area surrounded by the groove, whereas, outside this area, it decreases linearly up to the ambient pressure P_a. The pressure P_0 is identified as a function of P_2 and h, where h is expressed in [μm]:

$$P_0 = f\;\,(P_2 - P_a) + P_a = \left(1 - c_1{}^{\left(\frac{c_2}{h}\right)}\right)(P_2 - P_a) + P_a \tag{7}$$

A good identification of P_0 is obtained with c_1= 0.14; c_2= 5 μm. Integrating the pressure distribution under the pad, the correspondent pressure force F_p results equal to:

$$F_p = S_{eq}\,(P_0 - P_a);\; S_{eq} = \frac{1}{3}\left[ab + AB + \frac{(Ab + aB)}{2}\right] \tag{8}$$

The dynamic behavior of the pad is studied by linearizing the equations of the model through the perturbation method. The expressions of the mass flow rates, continuity equations and Equation (4) are linearized around a neighbour of a static equilibrium position of the air pad and their variations are expressed in Laplace domain. Also, equations (1), (8) are expressed in Laplace domain.

$$\begin{aligned}
&\overline{G_1} = k_1\overline{x} + k_2\overline{P_1};\; \overline{G_2} = k_3\overline{P_1} + k_4\overline{P_2} + k_5\overline{h};\\
&\overline{G_3} = k_6\overline{P_0} + k_7\overline{h};\; \overline{G_1} - 4\overline{G_2} = k_8\, s\,\overline{P_1};\\
&4\overline{G_2} - \overline{G_3} = k_9\, s\,\overline{h} + k_{10}\, s\,\overline{P_0};\\
&\overline{P_0} = k_{11}\,\overline{P_2} + k_{12}\,\overline{h};\\
&\overline{x} = k_{13}\,\overline{P_1};\; \overline{F_p} = S_{eq}\overline{P_0}
\end{aligned} \tag{9}$$

where:

$$k_1 = \left.\frac{\partial G_1}{\partial x}\right|_0 = \psi\pi d_V c_{da,1} P_S \sqrt{1-{\varphi_1}^2}\;\; ;\varphi_1 = 0 \quad \text{if} \;\; \frac{P_1}{P_S} \le b_c$$

$$\begin{aligned}
&k_1 = \left.\frac{\partial G_1}{\partial x}\right|_0 = 0 \;\text{ if }\; x < x_{min};\\
&k_2 = \left.\frac{\partial G_1}{\partial P_1}\right|_0 = -\frac{C_1}{1-b_c}\frac{\varphi_1}{\sqrt{1-{\varphi_1}^2}};\\
&k_3 = \left.\frac{\partial G_2}{\partial P_1}\right|_0 = C_2\left(\sqrt{1-{\varphi_2}^2} + \frac{P_2}{P_1}\frac{1}{1-b}\frac{\varphi_2}{\sqrt{1-{\varphi_2}^2}}\right);\; \varphi_2 = 0 \quad \text{if} \;\; \frac{P_2}{P_1} \le b_c\\
&k_4 = \left.\frac{\partial G_2}{\partial P_2}\right|_0 = -\frac{C_2}{1-b_c}\frac{\varphi_2}{\sqrt{1-{\varphi_2}^2}}\\
&k_5 = \left.\frac{\partial G_2}{\partial h}\right|_0 = \psi\,\pi d\, c_{da,2}\, P_1\sqrt{1-{\varphi_2}^2};\\
&k_6 = \left.\frac{\partial G_3}{\partial P_0}\right|_0 = \frac{P_0}{3\,\mu\,RT}\upsilon h^3;\\
&k_7 = \left.\frac{\partial G_3}{\partial h}\right|_0 = \frac{\upsilon\, h^2}{6\,\mu\,RT}\left[2P_0(P_2 - P_a)\frac{df}{dh}h + 3({P_0}^2 - P_a^2)\right];\\
&k_8 = \frac{V_1}{R\,T};\; k_9 = \frac{P_0\,A\,B}{R\,T};\;\; k_{10} = \frac{V_0}{R\,T};\, k_{11} = f;\\
&k_{12} = (P_2 - P_a)\frac{df}{dh};\;\; \frac{df}{dh} = \frac{c_2}{h^2}\cdot {c_1}^{\frac{c_2}{h}}\cdot ln\, c_1 \;\;;\;\; k_{13} = k_V
\end{aligned} \tag{10}$$

It is worth noting that, the exponential term of $c_{da,2}$ has been considered constant in computing the partial derivative of G_2 with respect to h. Making use of equations (9), it is possible to compute the transfer function $\overline{F_P}$ / $\overline{h}$:

$$H(s) = \frac{\overline{F_P}}{\overline{h}} = \frac{a_0}{b_0}\, S_{eq}\, \frac{1 + (a_1/a_0)\, s + (a_2/a_0)s^2}{1 + (b_1/b_0)\, s + (b_2/b_0)s^2} = K_S\, \frac{1 + \tau_1 s + \tau_2 s^2}{1 + \gamma_1 s + \gamma_2 s^2} \tag{11}$$

where:

$$a_0 = 16\,(k_3k_4k_{12} - k_3k_5k_{11}) - k_{11}(k_1k_{13} + k_2 - 4k_3)\left(4k_5 - k_7 - \frac{4k_4k_{12}}{k_{11}}\right);$$
$$a_1 = k_9k_{11}(k_1\,k_{13} + k_2 - 4k_3) + k_8k_{11}(4k_5 - k_7 - \tfrac{4k_4k_{12}}{k_{11}});$$
$$a_2 = -\mathrm{k_8k_9k_{11}};$$
$$b_0 = 16\,\mathrm{k_3k_4} - \mathrm{k_{11}(k_1k_{13} + k_2 - 4k_3)}\left(\mathrm{k_6} - \tfrac{\mathrm{4k_4}}{\mathrm{k_{11}}}\right);$$
$$b_1 = k_8k_{11}\left(k_6 - \frac{4k_4}{k_{11}}\right) - k_{10}k_{11}(k_1k_{13} + k_2 - 4k_3);$$
$$b_2 = k_8k_{10}k_{11};$$

$K_S = \frac{a_0}{b_0}\,S_{eq}$ is the static stiffness of the air pad. By expressing the transfer function $H(s)$ in the frequency domain, the theoretical dynamic stiffness K and damping c of the air under the pad are computed as:

$$K(\omega) = -\,Re_H(\omega) = -K_S\frac{1 + (\tau_1\,\gamma_1 - \tau_2 - \gamma_2)\omega^2 + \tau_2\,\gamma_2\,\omega^4}{(1 - \gamma_2\omega^2)^2 + (\gamma_1\omega)^2}$$
$$c(\omega) = -\,\frac{Im_H(\omega)}{\omega} = -K_S\frac{(\tau_1 - \gamma_1) + (\tau_2\,\gamma_1 - \tau_1\,\gamma_2)\omega^2}{(1 - \gamma_2\omega^2)^2 + (\gamma_1\omega)^2} \tag{12}$$

The equilibrium equation of the pad is:

$$\bar{F} - \bar{F_p} + Ms^2\bar{h} = 0 \tag{13}$$

where F is the vertical external load applied to the pad and M the mass related to the supported payload ($F = Mg$). By defining $G(s) = -\frac{1}{Ms^2}$, it is possible to obtain the closed loop block diagram of Figure 4. The equivalent transfer function of the entire system is:

$$G_{eq}(s) = \frac{G(s)}{1 + G(s)H(s)} = \frac{1}{K_S}\,\frac{(1 + \gamma_1 s + \gamma_2 s^2)}{(1 + \delta_1 s + \delta_2 s^2 + \delta_3 s^3 + \delta_4 s^4)} = \frac{\bar{h}}{\bar{F}} \tag{14}$$

$$\delta_1 = \tau_1\,;\ \delta_2 = \tau_2 - \frac{M}{K_S}\,;\ \delta_3 = -\frac{M\gamma_1}{K_S}\,;\ \delta_4 = -\frac{M\gamma_2}{K_S}$$

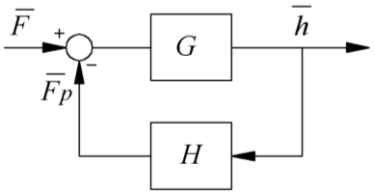

Fig. 4. Scheme of the feedback system.

5 Numerical results

5.1 Static analysis

The static load capacities of the compensated air pad with different parameters x0, dv, d, km are analysed. Table 1 shows the selected parameters in few different operative cases. Figure 5a shows the load capacity versus the air gap height. The comparison of the results for the compensated and the commercial air pads is made with the same supply pressure P_S = 0.5 MPa.

Table 1. Operative cases for compensated and commercial air pad

		x_0 (μm)	d_v (mm)	d (mm)	k_m (N/mm)
Compensated air pad	case a	-20	0.5	1	180
	case b	-20	0.5	0.18	180
	case c	-20	0.5	0.18	270
	case d	-20	0.5	1	270
	case e	-30	0.5	1	180
Commercial air pad	case f	-	-	0.18	-

Compared to the commercial air pad, the controlled one globally presents a lower load capacity but it exhibits a significantly higher stiffness. Moreover, as discussed in [12], due to the regulating action of the valve, the characteristic curves of the compensated pad can be divided in three different regions (Fig. 5b): a by-pass (A-B), compensation (B-C) and a saturation zone (C-D). When the system is lightly loaded (by-pass), the distance between the nozzle and the diaphragm is quite small and compensated pad behaves has a lumped pneumatic resistance ($x = x_{min} = x_{by-pass}$). As the load increases, the pressure in the valve chamber increases, the valves start regulating when $x > x_{by-pass}$ (compensation zone).

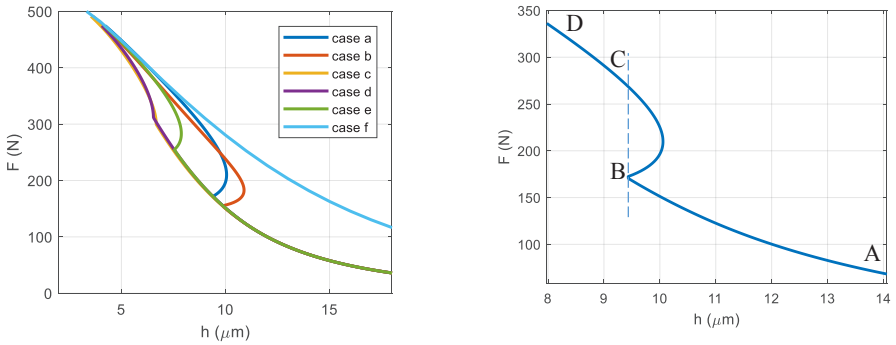

Fig. 5. a) Static load vs. air gap height, Ps = 0.5 MPa, commercial and compensated pads; b) A-B: by-pass zone, B-C: compensation zone, C-D: saturation zone.

Here, the compensating action of the valve makes it possible to compensate the air gap variations due to the change of the external load by increasing the air flow supplied to the pad. Beyond point C ($h_C = h_B$) the compensation is no more able to provide a suitable amount of air flow to compensate for air gap height variations. As can be seen, given the pad features, the characteristic shape of the load capacity curve is significantly influenced by the design parameters of the valve (x_0, d_v, and k_m). On this regard, Colombo et al. proposed a design

methodology to select the values of x_0, k_m that maximize the stiffness of the system at a desired air gap height [14]. Curve a) of figure 5 corresponds to the design condition of the control system.

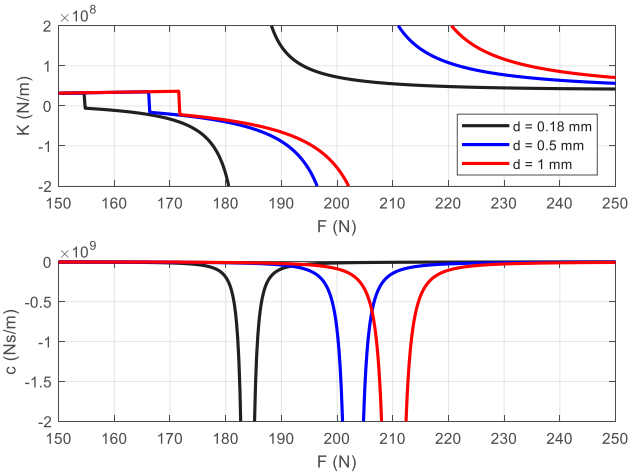

Fig. **6**. Stiffness and damping of the compensated pad in static conditions, for some diameters *d*: P_S = 0.5 MPa, x_0 = − 20 μm, d_v = 0.5mm, k_m =1.8 10^5 N/m.

Figure 6 shows the trends of the air pad stiffness K and the damping coefficient c obtained from equation (12) in static conditions (ω = 0). The trends of the static stiffness expressed as functions of the external payload F are reported by considering different sizes of the supply hole diameters of the compensated pad (d = 0.18, 0.5, 1 mm). It can be seen that, the stiffness changes sign in the regulation zone and it locally assumes values that tend to infinity, even c tends to infinity when K_S tends to infinity.

5.2 Dynamic analysis

The analysis of the dynamic behaviour is aimed at investigating the stiffness and damping values of the air gap as the frequency ω of the applied load F varies. The results are obtained with the design parameters (P_S = 0.5 MPa, x_0 = − 20 μm, d_v = 0.5mm, d = 1 mm, k_m =1.8 10^5 N/m, V_1 =1.4 10^{-6} m^3), moreover the investigations regard the air gap height values belonging to the compensation region. Figure 7 shows the trends of the dynamic stiffness and damping in the presence of different air gap heights within the regulation zone. Figure 7a shows the results for frequencies till to 100 Hz, figure 7b shows better the same results in the range of frequency from 10 Hz to 50 Hz. These results can be compared to those of figure 8 where the frequency response of the commercial pad is shown [15]. As can be seen, the stiffness and damping of the compensated pad reduce with the excitation frequency. In particular, both stiffness and damping drastically reduces even at low frequencies: at about 2 Hz, the stiffness halves and the damping reduces by 5 times. Meanwhile, the stiffness and damping of the commercial pad present two opposite trends with respect to the excitation frequency. The stiffness increases, whereas the damping reduces. Figure 9 shows the effect of the volume V_1 of the connecting ducts between valve and pad. Here, it is possible to see that increasing the volume V_1 makes reduces the compensating action of the valve.

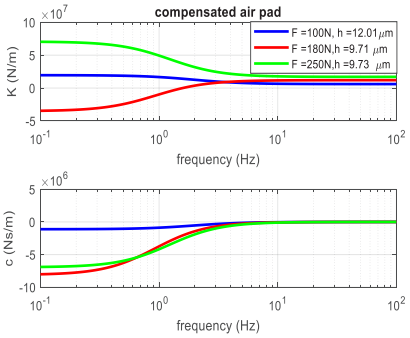

Fig. 7a. Compensated pad: dynamic stiffness and damping vs. frequency (from 0.1 Hz to 100 Hz). P_S = 0.5 MPa, $x_0 = -20$ μm, d_v = 0.5 mm, k_m =1.8 10^5 N/m, $V_1 = 1.4 \cdot 10^{-6}$ m^3

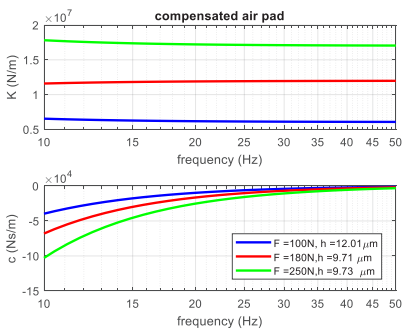

Fig. 7b. Compensated pad: dynamic stiffness and damping vs. frequency (from 10 Hz to 50 Hz), P_S = 0.5 MPa, $x_0 = -20$ μm, d_v = 0.5 mm, k_m =1.8 10^5 N/m, $V_1 = 1.4 \cdot 10^{-6}$ m^3

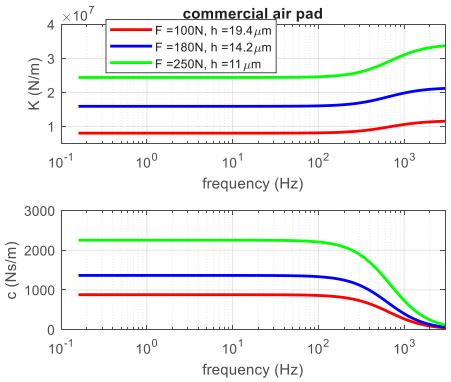

Fig. 8. Dynamic stiffness and damping vs. frequency for commercial pad, P_S = 0.5 MPa, d = 0.18 mm

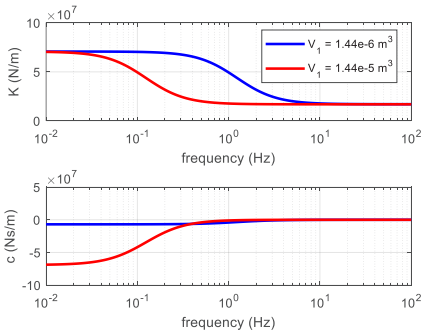

Fig. 9. Compensated pad. Dynamic stiffness and damping vs. frequency, effect of the volume V_1. P_S = 0.5 MPa, $x_0 = -20$ μm, d_v = 0.5 mm, d = 1mm, k_m =1.8 10^5 N/m, F= 250 N, h = 9.73 μm

5.3 Stability analysis

The dynamic results shown are related to the design operative condition of the pad. Both experimentation and simulations confirm stable operation in this situation. However, the controlled pad may not be stable in other working conditions. The stability is then theoretically analyzed by applying the Routh-Hurwitz criterion to the transfer function G_{eq}. The stability of the controlled air pad requires that all the coefficients δ_1, δ_2, δ_3, δ_4 must be positive. Moreover, the following two conditions (15) must be also satisfied:

$$f_1 = \delta_2 - \frac{\delta_1 \, \delta_4}{\delta_3} > 0 \; ; \; f_2 = \delta_1 - \frac{\delta_3}{f_1} > 0 \tag{15}$$

The stability of the system is evaluated by modifying the design parameter of the system ($P_S, x_0, d_v, d, k_m, V_1$) with respect to a stable operation selected as reference (case a of Figure 5). According to the Routh-Hurwitz method, the stability is evaluated by considering the signs of the coefficients δ_1, δ_2, δ_3, δ_4 and the functions f_1, f_2. In all the examined cases, the coefficients δ_1, δ_2, δ_3, δ_4 and the function f_1 are always positive while the function f_2

can assume negative values. Figures 10-14 show the fields of instability (gray areas) identified in this study. The stability maps are reported as functions of the load capacity. The range of load within which the behavior is observed includes the zone of normal operation of the air pad. It was found that, the system can become unstable in several cases: as the distance x_0 increases (or as d_v increases), as d increases, as k_m decreases, as V_1 decreases, as P_S increases. The unstable operating zones enlarge when the variation of the parameters increases with respect to the values relating to a stable operating condition.

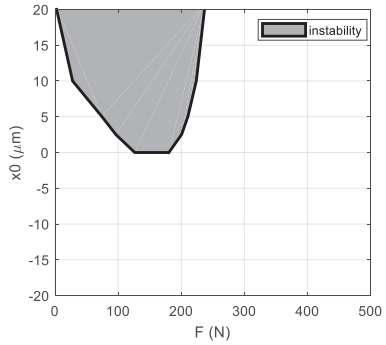

Fig. **10**. Stability map as x_0 varies: P_S = 0.5 MPa, d_v = 0.5 mm, d = 1mm, k_m =1.8 10^5 N/m, V_1 =1.4 10^{-6} m^3

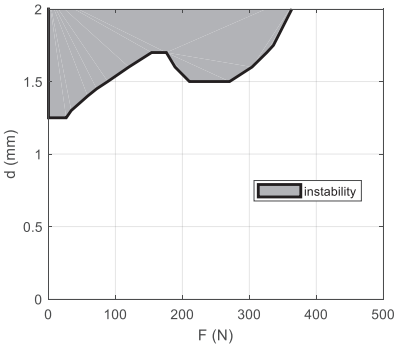

Fig. 11: Stability map as d varies: P_S = 0.5 MPa, $x_0 = -20$ μm, d_v= 0.5 mm, k_m =1.8 10^5 N/m, V_1 =1.4 10^{-6} m^3

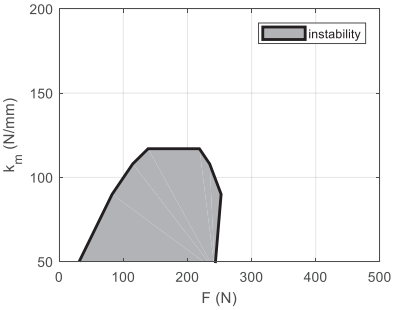

Fig. **12**. Stability map as k_m varies: P_S = 0.5 MPa, $x_0 = -20$ μm, d_v = 0.5 mm, d = 1mm, V_1 =1.4 10^{-6} m^3

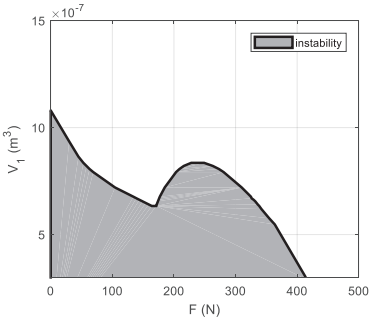

Fig. 13. Stability map as V_1 varies: P_S = 0.5 MPa, $x_0 = -20$ μm, d_v = 0.5 mm, d = 1mm, k_m =1.8 10^5 N/m.

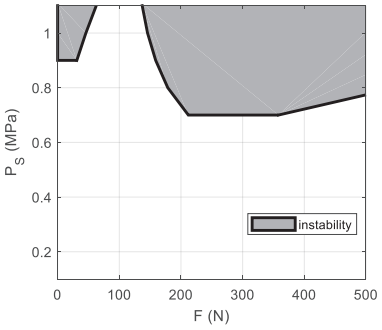

Fig. **14**. Stability map as P_S varies: $x_0 = -20$ μm, d_v = 0.5 mm, d = 1mm, k_m=1.8 10^5 N/m, V_1 =1.4 10^{-6} m^3

6 Conclusion

The present paper presented a numerical analysis of the dynamic behavior and stability of an aerostatic pad controlled by a diaphragm valve. The numerical model has been linearized to investigate the dynamic stiffness and damping of the compensated air pad. Within the regulating zone the static stiffness is significantly greater than that of the commercial air pad. Damping and stiffness decrease as the load application frequency increases and if the static operating point is very close to the point of infinite stiffness the dynamic stiffness is even greater than that of the commercial air pad. However, as the frequency varies, the damping remains much higher than that of the commercial pad.

The linearization of the model has made it possible to evaluate the stability of the system through the Routh-Hurwitz criterion. It has been found that the chosen design parameters allow a stable operation; the system is more prone to the instability at lower loads (higher air gap heights). However also the variation of the pad design parameters may lead to instability. In particular, the system can be unstable also at higher loads if the supply pressure increases. In fact, as the supply pressure increases, the instability field expands rapidly in almost the entire range of air gap heights. Moreover, it has been found that the system stability can be improved by increasing the volume of the ducts connecting the air pad to the valve, nevertheless, this also produces a significant reduction of the dynamic stiffness and damping. Ultimately, compared to the commercial air pad, the compensated one exhibit significantly higher performance for quasi-static applications.

Compared to other stability methods, Routh-Hurwitz criterion can be easily employed to verify the stability of dynamical systems and obtaining stability maps by considering different operating parameters of the investigated system. However, this method does not provide any information about the stability margin of the system. For this reason, feature works will be devoted to integrate the information related to the stability maps obtained through Routh-Hurwitz criterion with information regarding the stability margin of the investigated system, e.g., Nyqvist criterion. Moreover, these theoretical results will be verified through experiments.

References

1. Q. Gao, W. Chen, L. Lu, D. Huo, and K. Cheng, Tribology International (2019)
2. L. Lentini, M. Moradi, and F. Colombo, Tribology in Industry **40**, 165 (2018).
3. 3. D. A. Boffey, A. E. Duncan, and J. K. Dearden, *Tribology International* **14**, 287 (1981).
4. S. Z. Kassab, E. M. Noureldeen, and M. A. Shawky, *Tribology International* **30**, 533 (1997).
5. F. Colombo, L. Lentini, T. Raparelli, A. Trivella, and V. Viktorov, *Tribology Letters* **66**, (2018).
6. T. Nakamura and S. Yoshimoto, Tribology International **29**, 145 (1996).
7. A. Charki, K. Diop, S. Champmartin, and A. Ambari, *International Journal of Mechanical Sciences* **72**, 28 (2013).
8. M. Fourka and M. Bonis, *Wear* **210**, 311 (1997).
9. T. S. Luong, W. Potze, J. B. Post, R. A. J. Van Ostayen, and A. Van Beek, *Tribology International* **37**, 825 (2004).
10. F. Al-Bender, Precision Engineering **33**, 117 (2009).
11. T. Raparelli, V. Viktorov, F. Colombo, and L. Lentini, *Precision Engineering* **44**, 1 (2016).
12. D. Ghodsiyeh, F. Colombo, L. Lentini, T. Raparelli, A. Trivella, and V. Viktorov, *Tribology International* **141**, (2020).

13. G. Belforte, T. Raparelli, V. Viktorov, and A. Trivella, *Tribology International* **40**, 512 (2007).
14. F. Colombo, L. Lentini, T. Raparelli, A. Trivella, and V. Viktorov, *Lubricants* **9**, 47 (2021).
15. F. Colombo, L. Lentini, T. Raparelli, A. Trivella, and V. Viktorov, in *International Conference on Robotics in Alpe-Adria Danube Region* (Springer, 2018), pp. 678–686.